PALEOCEANOGRAPHY, VOL. 14, NO. 4, PAGES 542-558, AUGUST 1999

Late Ordovician glaciation under high atmospheric CO_2: A coupled model analysis

Pascale F. Poussart, Andrew J. Weaver, and Christopher R. Barnes

School of Earth and Ocean Sciences, University of Victoria, Victoria, British Columbia, Canada

Abstract. The analysis of the geologic record has revealed a question concerning how the Late Ordovician glaciation could have occurred simultaneously with high CO_2 levels (10-18x). Sensitivity studies using a coupled atmosphere-ocean-sea ice model show that it is possible to maintain a permanent snow cover (which corresponds to 60% of all the glacial deposits found on Gondwana) under 10x CO_2 levels, warm fall/cool spring orbital parameters, a 4.5% reduction in solar luminosity, a length of day of 21.5 hours, and an enhanced snow/sea ice albedo of 0.3. A cold summer orbit experiment with 10x CO_2 and a reduced snow/sea ice albedo of 0.1 also sustains a permanent (albeit less extensive) snow cover. The geographic configuration of the Late Ordovician results in an up to ~42% increase in the global ocean poleward heat transport in the Southern Hemisphere relative to present-day and a significant asymmetry relative to the equator.

1. Introduction

Analysis of the geological, chemical, and paleontological records of the Ordovician System has revealed a question concerning how the Late Ordovician glaciation could have occurred simultaneously with high atmospheric CO_2 concentrations. The continental glaciation on Gondwana is now a well-documented event by the work of *Beuf et al.* [1971], *Hambrey and Harland* [1981], and others. In terms of its extent it is the third most important glacial period in the Phanerozoic (past 545 m.y.) and coincides with the second greatest mass extinction event for that time [*Sepkoski*, 1995].

The chronology and timing of the glaciation remain issues of contention. *Frakes et al.* [1992] argued from the spatial and temporal distribution of continental glacial deposits and glaciomarine sediments that glacial inception was initiated during the Caradoc (464 – 443 Ma) and reached its maximum during the Ashgill, more specifically during the Hirnantian Stage (~440 Ma). The major ice sheet then covered at least North-central and West Africa, which was centered near the South Pole. This is also supported by the stable isotope record [*Middleton et al.*, 1991; *Wang et al.*, 1997; *Veizer et al.*, 1999] and eustatic curves [*Ross and Ross*, 1992]. Event stratigraphy conducted in northwest Africa suggests three to four major growth phases of the continental ice cap from the late Caradoc through the Ashgill [*Barnes*, 1986]. Whereas the ice sheet probably began to retreat during the Llandovery (~438 Ma) and had disappeared completely by the end of the Wenlock (~421 Ma), smaller glacial centers developed in southern Africa and southern Brazil, apparently following the motion of Gondwana over the South Pole [*Caputo and Crowell*, 1985; *Caputo*, 1998]. On the basis of carbon and oxygen isotopic data derived from an Ordovician-Silurian boundary interval, as well as bathymetric evidence, *Brenchley et al.* [1995] argued for a short-lived glaciation (0.5 m.y.). Additional support for this alternative hypothesis has come from the precise dating of North African glacial deposits of Hirnantian age by *Paris et al.* [1995], *Marshall et al.* [1997], and *Underwood et al.* [1997].

The spatial distribution of Late Ordovician glacial deposits on Gondwana suggests that land-based ice spread outward to at least 40°S. The floating ice may have extended 10° farther equatorward [*Brenchley and Newall*, 1984]. Estimates of the size of the ice sheet vary from 6-8 x 10^6 km^2 [*Beuf et al.*, 1971; *Hambrey*, 1985] to 11.8 x 10^6 km^2 when accounting for some erosion [*Crowley and Baum*, 1991].

Evidence for high atmospheric CO_2 has stemmed mainly from the study of paleosols and geochemical modeling experiments. The analysis of goethites from an ironstone in the Upper Ordovician Neda Formation and potentially contemporaneous to the glaciation has yielded an atmospheric pCO_2 estimate of ~20x preindustrial levels (pil = 280 ppm) [*Yapp and Poths*, 1992]. These estimates are also supported by geochemical modeling experiments that predicted atmospheric pCO_2 levels ~14 ± 6x pil [*Berner*, 1994]. However, Berner's estimates may not be simultaneous to a glaciation confined to the Hirnantian since the model has a time step of 10 m.y. In addition, as pointed out by *Kasting* [1992], the large uncertainties associated with geochemical estimates of pCO_2 challenges the existence of a CO_2-glaciation paradox. The carbon isotope compilations provided by *Brenchley et al.* [1995] and *Paris et al.* [1995] reveal a distinct positive shift at the end of the Ordovician, which suggests a significant change in the mode of carbon cycling. The widespread distribution of this shift in the latest Ordovician suggests that it was of global significance and that it may have had a common origin. *Wang et al.* [1993] proposed that a decrease in pCO_2 in the ocean or in the atmosphere, together with a greater organic carbon burial rate during the Hirnantian, might have caused the positive shift. Higher than usual organic carbon burial rates may be expected during glacial times. If CO_2 levels were relatively low for a short period of time simultaneous to the glacial maxima, as surmized from the positive shift of the carbon isotope [*Wang et al.*, 1993;

Copyright 1999 by the American Geophysical Union.

Paper number 1999PA900021.
0883-8305/99/1999PA900021$12.00

Brenchley et al., 1995], the climatic conditions that led to the glacial inception may still have included CO_2 concentrations 8-20x pil.

The occurrence of the Late Ordovician glaciation simultaneous with high CO_2 levels has been addressed previously through several modeling analyses. *Crowley et al.* [1987] showed through energy balance model (EBM) experiments that the unique geographic configuration of Gondwana (with the South Pole in a coastal location) could have allowed for permanent snow cover with higher CO_2 levels. Subsequent experiments, which included nonlinear ice-albedo feedbacks, gave further support to the geographic positioning hypothesis [*Hyde et al.*, 1990; *Crowley and Baum*, 1991]. However, because the timescales involved in tectonic processes are incompatible with a short-lived Hirnantian glaciation, it is evident that the particular geographic configuration of Gondwana is a necessary but not sufficient condition for the growth and decay of the Gondwana ice cap. *Crowley and Baum* [1991] found that by prescribing a 3.5-5.0% decrease in solar luminosity [*Endal and Sofia*, 1981] and a realistic Ordovician geography, the EBM sustained permanent ice when driven by a 7-13x CO_2 forcing. As an extension to their previous analysis, *Crowley and Baum* [1995] used the Global Environmental and Ecological Simulation of Interactive Systems (GENESIS) atmospheric general circulation model (AGCM) 1.02A with a specified mixed layer slab ocean [*Thompson and Pollard*, 1995], CO_2 levels 14x pil, -4.5% solar luminosity, and an orbital configuration prescribed for minimum summer insolation receipt (cold summer orbit (CSO)). They focused on the effects of different combinations of ocean heat transport (1x versus 1.5x meridionally symmetrized heat transport based on a present-day control experiment) and topography (300-500 m) on high-latitude snow cover over Gondwana. They showed that in the elevated topography case (500 m), permanent snow cover was found where the geological record indicated the Ordovician ice sheet was present. *Gibbs et al.* [1997] examined the sensitivity of the Late Ordovician climate to variations in atmospheric CO_2 using the GENESIS AGCM and found that a "runaway icehouse" occurred with 8x CO_2 levels, whereas for the 10x experiment, a snow cover coincident with the distribution of glacial deposits survived through the summer. There was no permanent snow cover in the 18x experiment.

Here we conduct a series of sensitivity studies with an energy/moisture balance model (EMBM) coupled to an ocean general circulation model (OGCM) and to a thermodynamic sea-ice model. The work presented here is complementary to previous AGCM experiments as we now emphasize the ocean's role in influencing the Late Ordovician climate. Advantages stemming from the use of the coupled OGCM-EMBM include a direct estimate of ocean heat transports as well as the inclusion of ocean-atmosphere feedbacks, which would be ignored in an ocean-only model. The use of the computationally efficient EMBM also allows for the assessment of a wide range of parameters, which have not been previously addressed. These include the effect of orbital configurations intermediate between hot and cold summer orbits and the sensitivity to the magnitude of the sea-ice/snow feedback parameter.

The remainder of this paper is structured as follows: section 2 provides an overview of the coupled model; section 3 presents the Late Ordovician control climatic response; section 4 addresses the sensitivity of the coupled model to changes in atmospheric CO_2 (section 4.1), orbital parameters (section 4.2), and sea-ice/snow albedo feedback (section 4.3); section 5 provides a discussion of the results; and section 6 contains concluding remarks.

2. The Coupled Model

The atmospheric component of the coupled model is the EMBM developed by *Fanning and Weaver* [1996]. The model includes a representation of the thermodynamic and hydrological components of the climate system and is based on the vertically integrated energy-moisture equations, with advection parameterized using an eddy-diffusive approach. The EMBM assumes no heat or water storage on land, so that surface latent and heat fluxes are zero there. Precipitation occurs whenever the relative humidity is >85%, falling as snow whenever the surface air temperature (SAT) is below -10°C. Over land, snowfall is redistributed in order to cover the entire grid cell, whereas over sea-ice a fractional area is permitted. An ice-albedo feedback is included whenever sea-ice is present and whenever the SAT over land is below -10°C through the local reduction of the latitudinal profile of the planetary coalbedo by 0.1 [*Graves et al.*, 1993] as in *Fanning and Weaver* [1996] and *Weaver et al.* [1998]. When atmospheric temperatures rise above -10°C, the snow melt rate linearly increases from 0 to 5 cm d^{-1} at 0°C.

The EMBM was coupled to the Geophysical Fluid Dynamics Laboratory modular ocean model [*Pacanowski*, 1995] through latent, sensible, and radiative heat transfers at the air-sea interface (the ocean component is discussed in detail by *Weaver and Hughes* [1996]). A simplified thermodynamic sea-ice model based on *Semtner* [1976] and *Hibler* [1979] was also included and is detailed by *Fanning and Weaver* [1996]. Over sea-ice, surface fluxes due to longwave and shortwave radiative forcing, as well as sensible and latent heat exchanges, were balanced by the conduction of heat through the ice and the heat absorbed because of ice melt.

The advantages gained from using the EMBM arise from its simplicity, computational efficiency, and freedom from explicit flux adjustments. The later allows for the investigation of past climates differing from the present-day. Coupled model experiments provide an adequate representation of the present-day climate and compare favorably with paleoclimatic data [*Fanning and Weaver*, 1997; *Weaver et al.*, 1998]. However, the simple parameterization of the diffusive moisture transport causes global precipitation rates to be too low compared to present-day observations. Precipitation patterns also fail to reproduce the belt of high precipitation associated with the Intertropical Convergence Zone. While the EMBM has numerous deficiencies [see *Fanning and Weaver*, 1996], it is a useful tool for process-oriented coupled ocean-atmosphere studies such as the one conducted here. In the following subsections we describe the deviation of the present version of this coupled model from that described by *Fanning and Weaver* [1996] and *Weaver et al.* [1998].

2.1. Land-Sea Distribution

The land-sea distribution is derived from the one used by *Crowley and Baum* [1995]. Since there was no reconstruction available for the Late Ordovician, Crowley and Baum modified

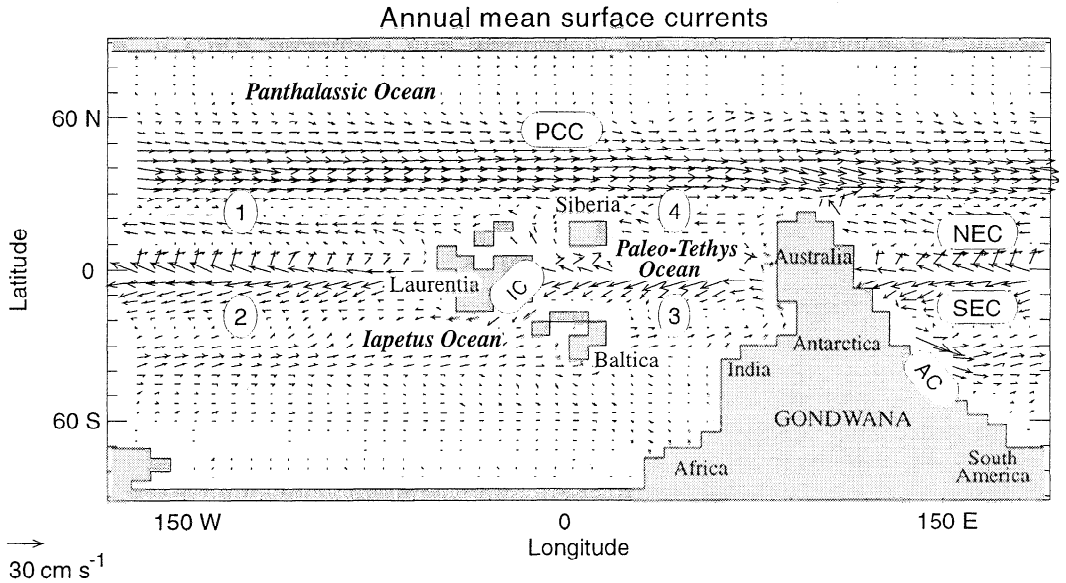

Figure 1. Annual mean surface velocities (cm s^{-1}) obtained from Ordovician control experiment. Ovals represent ocean gyres: (1) north Panthalassic convergence, (2) south Panthalassic convergence, (3) south Paleo-Tethys convergence, and (4) north Paleo-Tethys convergence. Rounded rectangles represent surface currents: Panthalassic Circumpolar Current (PCC), Iapetus Current (IC), North and South Equatorial Currents (NEC, and SEC), and Antarctica Current (AC). Vectors are drawn every grid point for legibility.

the *Scotese and Golonka* [1992] reconstruction of the Silurian (Wenlock epoch, ~433 Ma) by rotating the landmasses 5° to the north. Gondwana's position was then tangential to the South Pole (Figure 1). For this study a linear interpolation was conducted on the original mask to correspond to the model's 3.75° zonal resolution and 1.8555° meridional resolution. From lack of geological evidence a flat-bottom topography was prescribed, with constant depth of 5400 m.

2.2. Earth's Rotation Rate

Estimates of the rotational deceleration of the Earth have been obtained from the paleontological analysis of stromatolites [*Scrutton*, 1978] and tidal rhythmites [*Sonett et al.*, 1996; *Williams et al.*, 1997]. The transfer of angular momentum to the moon's orbit causes the major axis of the moon's orbit to increase at the expense of the Earth's rotation rate. This has resulted in an appreciable increase in the length of day (LOD) through geologic time [*Sonett et al.*, 1988]. Here the Early Silurian LOD estimate of 21.5 hours was used [*Berger et al.*, 1989]. As such, we increased the Earth's rotation rate from 7.29×10^{-5} to 8.12×10^{-5} rad s^{-1}.

2.3. Orbital Parameters

The sensitivity of the coupled model to orbital parameters was investigated through a series of experiments using two extreme and two intermediate configurations. These configurations are defined as follows: a "hot summer orbit" (HSO) with an obliquity of 24.5°, an eccentricity of 0.06, and a longitude of perihelion of 270° (Figure 2b), a CSO (22.0°, 0.06, and 90°; Figure 2c), a "warm fall-cool spring orbit" (WFCS) (22.0°, 0.06, and 0°), and a "cool fall-warm spring orbit" (CFWS) (22.0°, 0.06, and 180°). For comparison, the present-day configuration is (23.47°, 0.0167, and 282°; Figure 2a). According to calculations conducted by *Berger et al.* [1989], changes in the Earth-moon distance, the Earth's rotation rate, and its moment of inertia during the Phanerozoic could have induced ~10% variations in precessional periods and ~20% variations in obliquity periods. However, the magnitude of the change in forcing is unknown. Hence the two extreme orbital configurations found for the Pleistocene were used [*Berger*, 1978].

2.4. Atmospheric CO_2

Experiments were conducted using CO_2 values of 10x, 14x, and 18x pil. These values are representative of the range of CO_2 estimates. The CO_2 radiative forcing is calculated as follows:

$$F = 5.77 \times 10^{3} \ln\left(\frac{CO_2}{350.0}\right)$$

This logarithmic relationship reflects the saturation of different CO_2 absorption bands at higher concentrations and gives a radiative forcing of 4 W m^{-2} for a doubling of CO_2 [*Ramanathan et al.*, 1987] and a climate sensitivity of 0.75°C W^{-1} m^2 [*Weaver et al.*, 1998].

2.5. Solar Luminosity

Studies on solar evolution have suggested a 25-40% increase in luminosity over the Earth's history [*Newman and Rood*, 1977; *Endal and Sofia*, 1981; *Bahcall*, 1988]. Late Ordovician estimates of solar luminosity imply a 3.5-5.0% decrease. These estimates depend on the definition of the original components of the Sun's core [*Crowley and Baum*, 1991]. Here, we used a 4.5% decrease as suggested by *Crowley and Baum* [1995] and hence a solar constant of 1.306×10^{3} W m^{-2}.

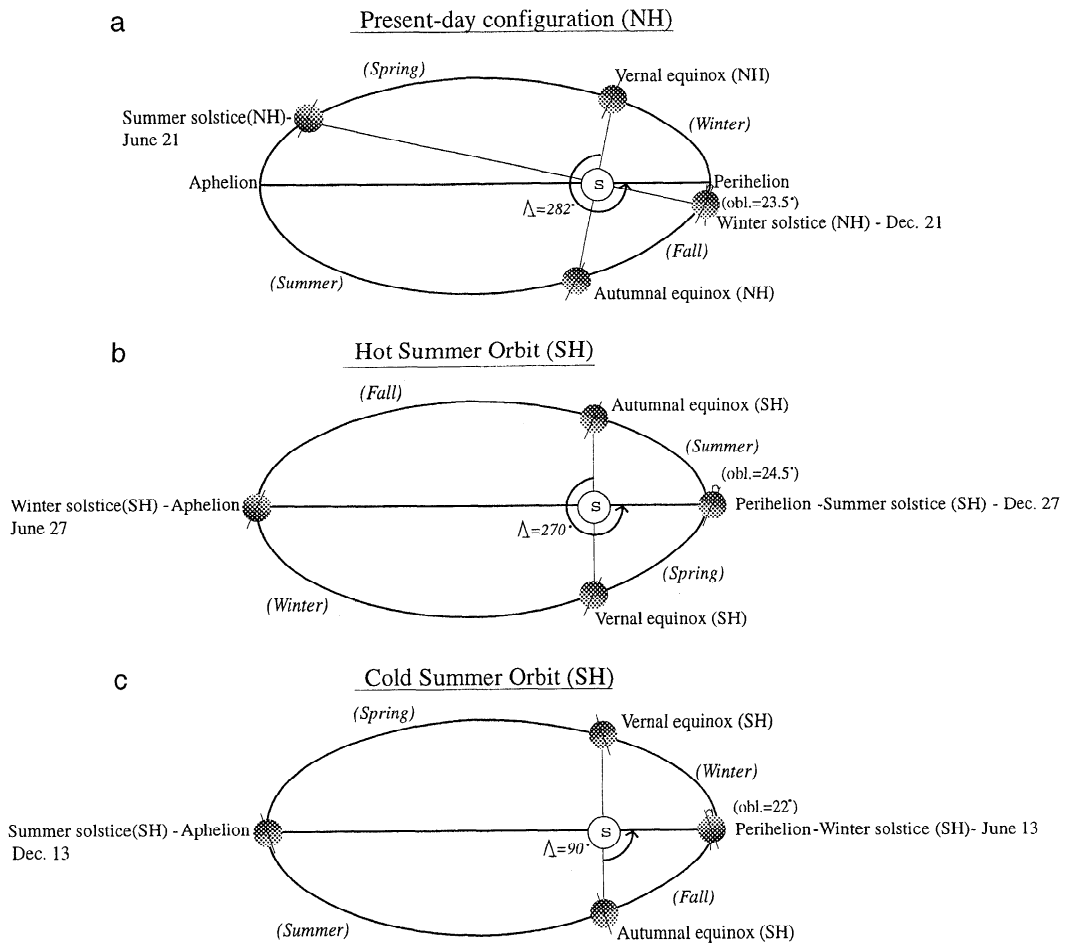

Figure 2. Sketch of the orbital configurations used in the modeling experiments: (a) present-day orbit (PDO), (b) hot summer orbit (HSO) for the Southern Hemisphere, (c) cold summer orbit (CSO) for the Southern Hemisphere. The longitude of the perihelion (Λ) is relative to the vernal equinox in the Northern Hemisphere. The eccentricity of orbit is not to scale.

2.6. Topography

There are currently no detailed topographic maps of the Ordovician Period. Hence a flat topography on the continents (at sea level) was prescribed. This is probably a realistic first-order approximation since during the Middle Ordovician, extensive epicontinental seas were covering parts of Gondwana, Laurentia, Baltica, and Siberia. In addition, because river drainage basins are unknown for this time period, we defined a river mask in which rain falling and snow melt on land is equally redistributed to all coastal land points.

2.7. Wind Fields

For this study we used monthly averaged wind fields previously generated with the GENESIS AGCM [*Gibbs et al.*, 1997]. The wind fields were obtained using an Ordovician geography [*Crowley and Baum*, 1995], 10x or 18x atmospheric CO_2 levels, CSO, 4.5% decrease in solar luminosity, and present-day LOD. For a complete description of the global climate model GENESIS, see *Thompson and Pollard* [1995]. From the geostrophic balance the wind speed fields were scaled everywhere outside 10°N and 10°S to account for the shorter LOD of 21.5 hours as follows:

$$(u_s, v_s) = \frac{f_{pd}}{f_o}(u_u, v_u) = 0.898\,(u_u, v_u)$$

where u_S and v_S (u_u and v_u) represent the scaled (unscaled) components of the wind speed and f_{pd} and f_o are the present-day and Ordovician Coriolis parameters. These wind speeds were used in the calculation of latent and sensible heat fluxes and converted to wind stress fields directly to drive the ocean. As suggested by *Jenkins et al.* [1993], the position of the Hadley/Ferrel/Polar cells would have been dramatically different during the Precambrian when the LOD was 14 hours. Our geostrophic modification of Gibbs winds is a good first-order approximation for small perturbations in LOD from present.

2.8. Changes in Albedo

The nature of the Earth's surface (vegetation cover, snow-ice cover, etc.) strongly influences the amount of solar radiation absorbed or reflected at the surface. Hence the albedo plays an important role in the energy balance. The model partially accounts for this mechanism by allowing the planetary coalbedo to decrease whenever snow/ice surfaces are present.

No parameterization is included for changes in albedo over land because of variations in vegetation cover and soil types or to the presence of epicontinental seas. The Ordovician Period occurred prior to the development of land plants, and knowledge of the geographic location of lakes is negligible. The sensitivity of the coupled model to changes in the magnitude of the ice-snow albedo feedback was tested by using three possible local reductions to the planetary coalbedo (0.1, 0.2, and 0.3) when sea ice/snow was present. The solar zenith angle effect, which is taken into account in the present-day estimate of 0.1 [*Graves et al.*, 1993], depends on the obliquity of the Earth. This parameter is likely to have varied throughout the Ordovician Period. In addition, the present-day coalbedo reduction is probably an underestimate for glaciated climates because there is a large difference in albedo between fresh (0.75-0.95) and old (0.40-0.60) snow [*Houghton*, 1985].

2.9. Initial Conditions

All experiments were conducted from resting state and integrated to equilibrium, which is defined as the time when the ocean mean heat flux has dropped below 10^{-2} W m^{-2}. Initial conditions for the ocean model included a simplified sea surface temperature (SST) distribution from *Levitus and Boyer* [1994] and globally constant salinity. The initial atmosphere was 0°C everywhere and contained no moisture.

3. Modeled Late Ordovician Control Climatic Response

We start our analysis by presenting results from the control experiment in which the orbital parameters (CFWS) describe a midpoint configuration between the HSO and CSO while the obliquity is kept to a minimum. This setting provides an appropriate representation of the average orbital forcing that would occur on timescales representative of the Late Ordovician glaciation. Results from all experiments discussed in this paper, as well as a description of their boundary conditions, are summarized in Table 1.

The modeled surface circulation patterns (Figure 1) compare favorably with the description provided by *Wilde* [1991]. Because of the absence of continental masses in the Northern Hemisphere, the wind stress field between 30° and 60°N induces a strictly zonal west-to-east surface circulation. Panthalassic waters confined to this latitudinal belt travel at speeds comparable to present-day values characteristic of the Antarctic Circumpolar Current (average = 24 cm s^{-1}), as they circle the globe unimpeded (Panthalassa Circumpolar Current). The east-to-west surface currents adjacent to the North Pole are weak as they are under persistent sea-ice. The presence of Laurentia, Baltica, Siberia, and northern Gondwana results in the formation of meridional flows at equatorial latitudes. Strong westward flowing equatorial currents straddling the equator exist between Laurentia and northern Gondwana. Laurentia and Siberia act as meridional barriers as they divert the North Equatorial Current northward and force the flow to join the North Paleo-Tethys ocean gyre. The South Equatorial Current travels freely across the Panthalassic Ocean until it reaches the Australian-Antarctic shield and becomes part of the western boundary Antarctica Current as it travels toward the South Pole. The second segment of the South Equatorial Current arises from the South China region and flows westward until the Avalonia-Baltica shield blocks it. Two major oceanic high-pressure gyres are present in the southern midlatitudes: the south Panthalassic gyre and the south Paleo-Tethys gyre. The two systems are linked through the Iapetus Current. The modeled annual mean sea surface salinity distribution (Figure 3) reveals the highest salinity values within 10°-30° north and south of the equator, where most of the evaporation takes place (not shown). Salinity values are minimum at polar latitudes where melting of sea-ice becomes important.

The SAT over Gondwana remains above freezing during the month of January (Figure 4b), whereas the spatial distribution of freezing atmospheric temperatures during the month of July

Table 1. Late Ordovician Modeling Results

Experiments	Int.	T_o	T_a	V_i(SH)	A_i(SH)	A_i(NH)	A_{sG}	*A>0.1*	*A>0.01*
Control (10x)	3000	1.4	12.6	470	0.93	20.4	0.00	0.00	0.00
10x_wfcs.1 (aj0.1)	4000	1.4	12.6	2530	2.83	16.2	0.17	0.11	0.12
10x_wfcs.2 (aj0.2)	2100	1.1	10.6	73000	7.26	23.9	4.13	1.45	3.88
10x_wfcs.3 (aj0.3)	2100	0.6	6.7	640500	17.70	59.4	14.5	13.70	14.30
10x_cso.1	3000	1.4	12.6	2645	2.90	17.3	0.54	0.41	0.42
10x_hso.1	3000	1.4	12.3	139	0.65	21.4	0.00	0.00	0.00
14x_cfws.1	3000	1.7	14.3	0	0.00	18.6	0.00	0.00	0.00
14x_wfcs.1	4000	1.7	14.5	260	0.65	14.5	0.00	0.00	0.00
18x_cfws.1	3000	1.7	15.3	0	0.00	16.2	0.00	0.00	0.00
18x_wfcs.1	4000	1.8	15.4	210	0.39	12.3	0.00	0.00	0.00
1x_pdo.1	4000	1.2	10.5	2900	1.45	45.7	---	---	---

The name of each experiment has three components: the first refers to the atmospheric CO_2 concentration (relative to 280 ppm), the second is the orbital configuration, and the third represents the magnitude of the ice-snow albedo parameter. Control (10x) is equivalent to 10x_cfws.1. Int. represents the integration time (years) required to reach equilibrium. All experiments except for the 1x_pdo.1 have a prescribed 21.5 hour length of day (LOD) and –4.5% solar luminosity. T_o is the depth-averaged global ocean equilibrium temperature (degrees Celsius); T_a is the annual mean equilibrium SAT (degrees Celsius); V_i(SH) represents the January mean sea-ice volume in the Southern Hemisphere (cubic kilometers), A_i(SH) is the January averaged sea-ice area in the Southern Hemisphere, and A_i(NH) is the July averaged sea-ice area in the Northern Hemisphere (x10^6 km^2). A_{sG} is the January averaged snow area on Gondwana and *A>0.1* and *A>0.01* are snow areas on Gondwana with thickness greater than 0.1 and 0.01 m, respectively (x10^6 km^2).

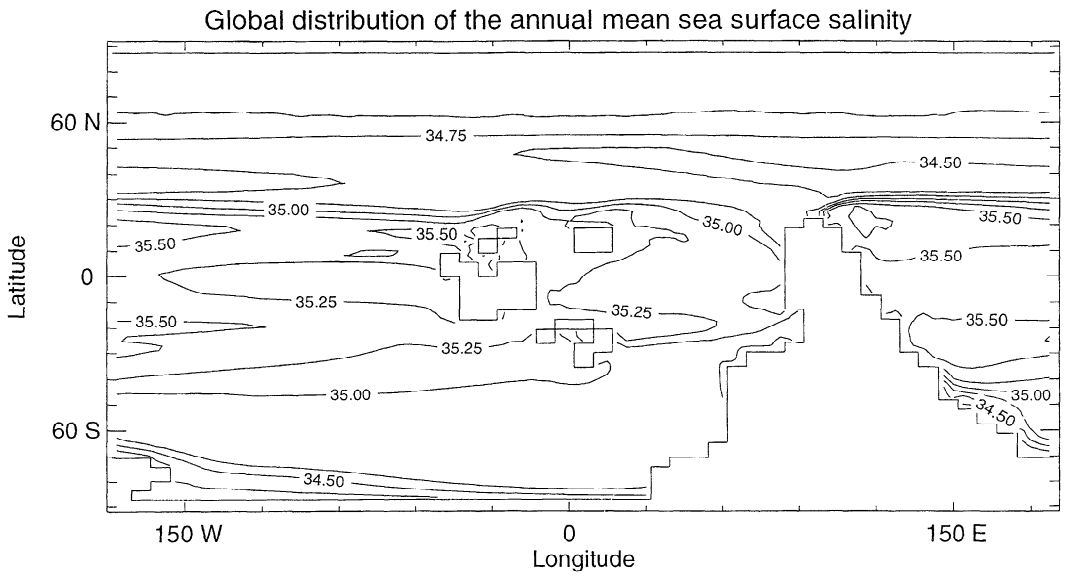

Figure 3. Global distribution of the annual mean sea surface salinity for control experiment in parts per thousand.

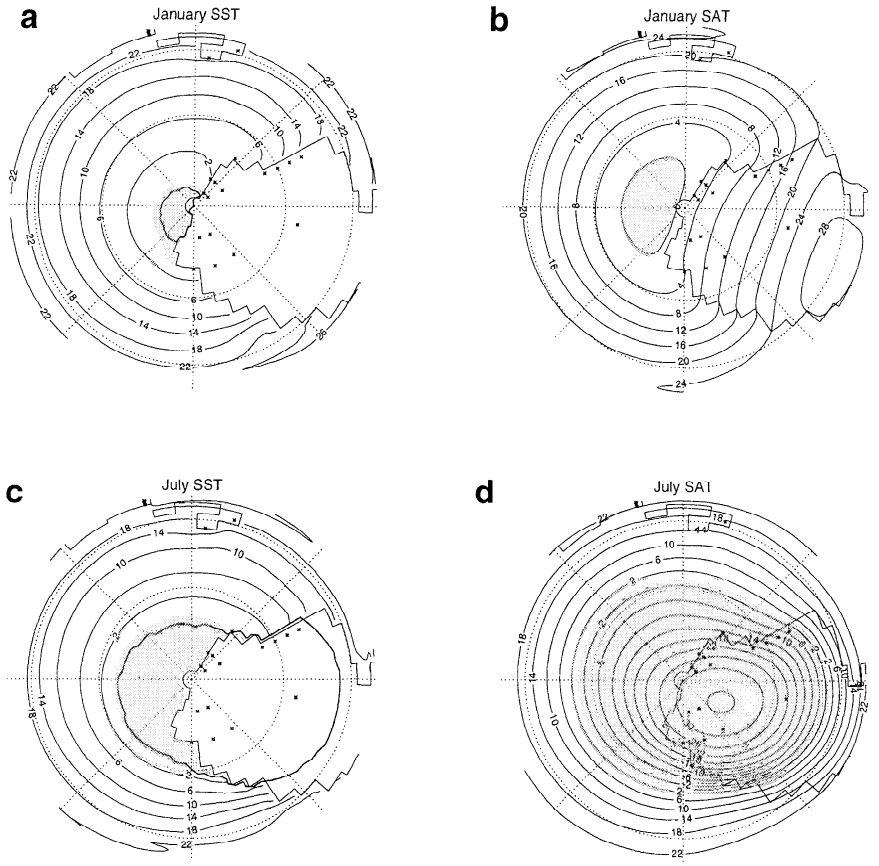

Figure 4. Modeled January and July sea surface temperature (SST) and surface air temperature (SAT) for control experiment (south polar orthographic projection). Asterisks represent an approximate distribution of glacial deposits [*Paris et al.*, 1995]. Contour intervals are 4°C. The heavy line over the ocean for SST graphs represents the maximum sea-ice extent, whereas over Gondwana it represents the location of the −10.0°C contour or the snow extent (whichever extends the farthest to low latitudes). The ice edge delimits the maximum snow/sea-ice-covered area present during the months of January or July. Shading indicates temperatures below 0°C.

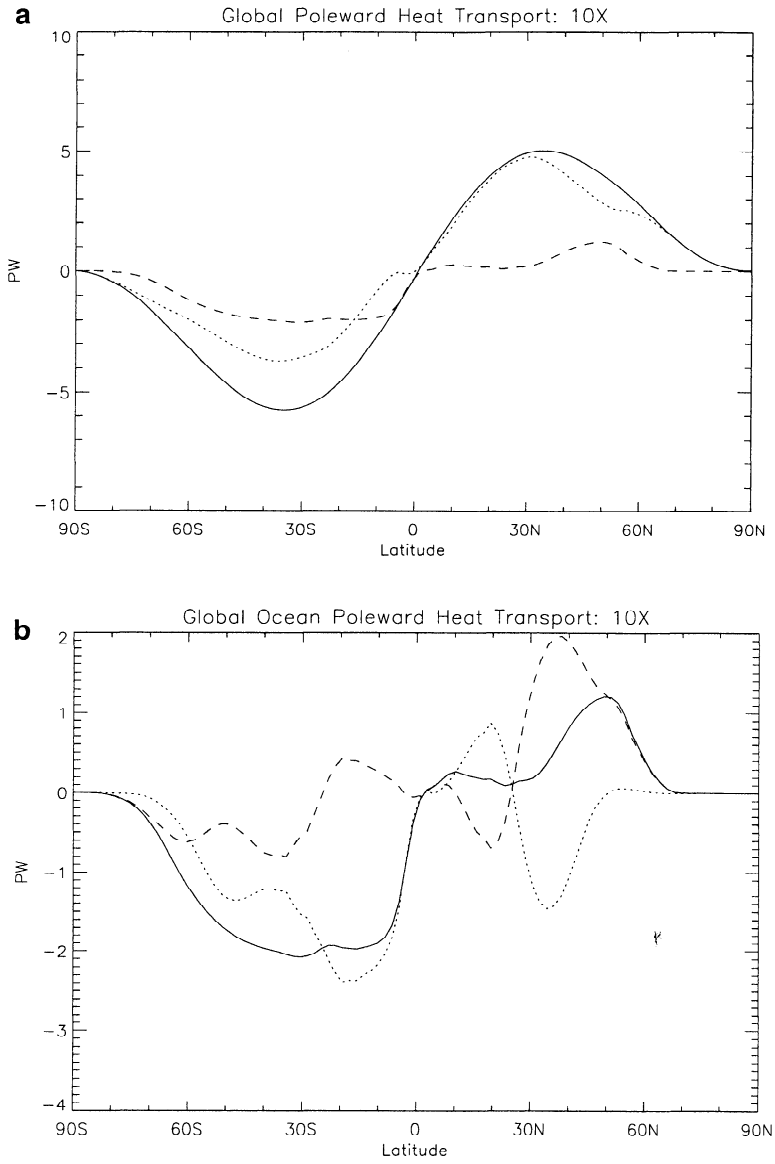

Figure 5. (a) Annual mean poleward planetary heat transport in Petawatts (PW) with ocean (dashed line) and atmosphere (dotted) components for the Ordovician control experiment, and (b) global ocean poleward heat transport for the Ordovician control experiment in PW. The three curves represent total (solid), advective (dotted line), and diffusive (dashed line) transports (1 PW=10^{15} W).

fully covers glacial deposits found on Gondwana (Figure 4d). SSTs cooler than −1.8°C, as depicted by the ice edge (Figures 4a and 4c), are located in the vicinity of the South Pole and coincide with the majority of the coastal glacial deposits. A permanent sea-ice cover exists in this control experiment, although permanent snow cover is not supported over Gondwana (Table 1).

The energy balance requirements imply that at equilibrium the annual and global mean incoming shortwave radiation balances the outgoing longwave radiation. The planetary heat transport ($T_{pl}(\phi)$), averaged across a line of latitude ϕ, is then calculated as follows:

$$T_{pl}(\phi) = \int_{\phi_s}^{\phi} [Q_{\text{in}} - Q_{\text{out}}] a \, d\phi'$$

where Q_{in} and Q_{out} are the zonally and annually averaged incoming shortwave and outgoing longwave radiation, a is the Earth's radius, and ϕ_s is the latitude of the southern boundary. The atmospheric heat transport is obtained by subtracting the ocean heat transport from $T_{pl}(\phi)$.

In the Northern Hemisphere the atmospheric contribution dominates the planetary transport at most latitudes, with a maximum of ~4.5 Petawatts (PW) near 30°N (Figure 5a). The ocean heat transport is important in the Southern Hemisphere and at midlatitudes in the Northern Hemisphere. The sole region for which the ocean dominates (with a maximum of ~2.1 PW at 10°S) is at low latitudes in the Southern Hemisphere. These low latitudes are regions of maximum top-to-bottom ocean potential temperature differences. In addition, the presence of a meridional land barrier allows for

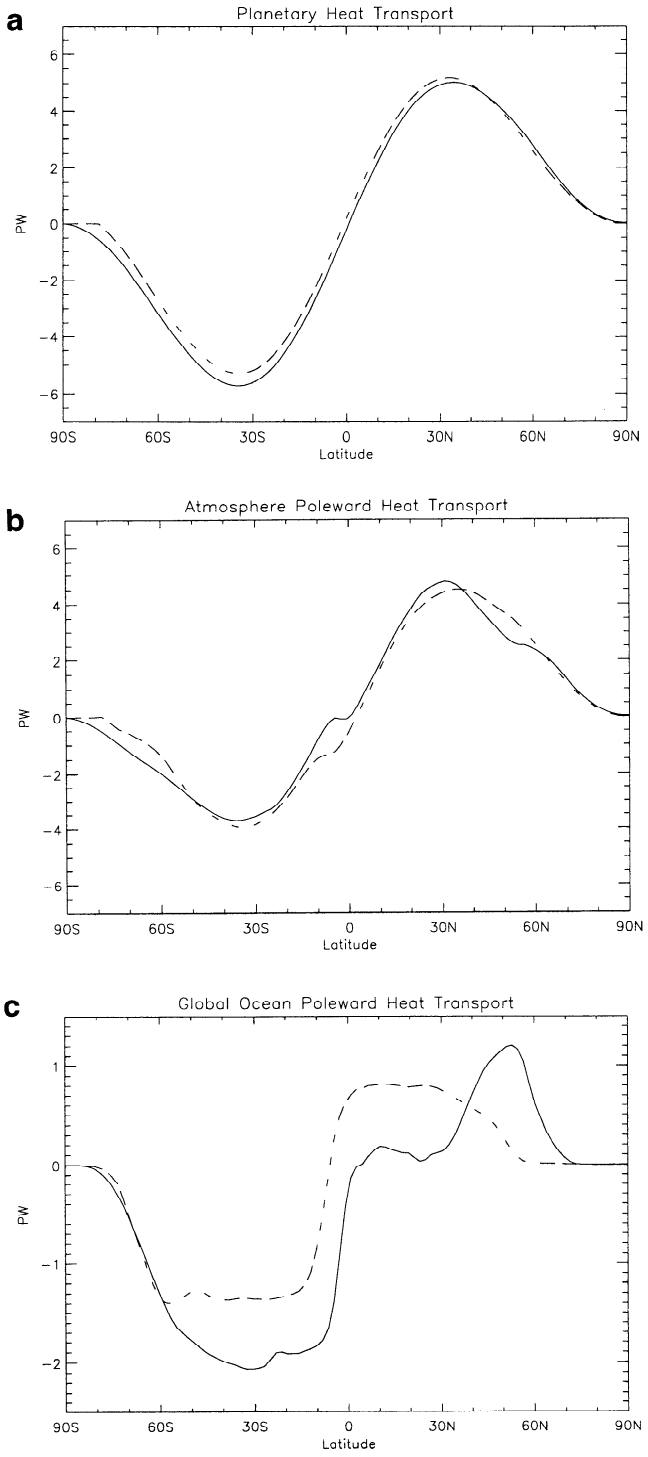

Figure 6. Heat transport comparison between the present-day run (dashed line) and the Ordovician control run (solid line) in PW: (a) planetary heat transport, (b) atmosphere poleward heat transport, and (c) global ocean poleward heat transport.

the existence of an intense western boundary current flowing along eastern Gondwana, the Antarctica Current (Figure 1).

The asymmetry of the total ocean heat transport curve indicates a more significant transport in the Southern Hemisphere than in its northern counterpart. In addition, the bulk of the heat transport is done by advection (Figure 5b, dotted line) via the Antarctica Current. Between the equator and 25°N the net oceanic heat transport is small as the northward advective Ekman transport counters the southward subsurface diffusive transport. As one moves northward of 25°N, most poleward heat transport is done by diffusion (Figure 5b, dashed line), whereas southward transport is done by advective Ekman transport.

For comparison purposes a "present-day" experiment was conducted using present-day geography, CO_2 levels, orbital parameters, solar luminosity, ice-snow albedo feedbacks, and LOD [*Wiebe and Weaver*, 1999]. The planetary heat transport peaks in midlatitudes with a maximum of ~5.0 PW in the Northern Hemisphere for both the present-day and Ordovician control experiments (Figure 6a). In the Southern Hemisphere the present-day peak transport (~5.5 PW) is slightly less than the Ordovician control experiment transport (~6.0 PW, Figure 6a). The atmospheric and oceanic components of the planetary heat transport for the present-day run (Figures 6b and 6c) agree favorably with observations [*Hartmann*, 1994], although differences are apparent. Because of the coarse resolution of the coupled model, the maximum ocean heat transports obtained from the present-day experiment (~0.8 PW in Northern Hemisphere and ~1.4 PW in Southern Hemisphere) are significantly smaller than that derived from observations [*Fanning and Weaver*, 1996].

The global ocean poleward heat transport increased by up to ~42% in the Southern Hemisphere between the present-day run and Ordovician control experiment and was shifted poleward in the Northern Hemisphere. Previous modeling experiments with the GENESIS AGCM coupled to a mixed layer slab ocean used a prescribed zonally symmetric ocean heat transport [*Crowley and Baum*, 1995; *Gibbs et al.*, 1997]. The two ocean heat transport schemes used were based on estimated present-day values (with a maximum transport of ~0.45 PW) and on a 50% increase (with a maximum transport of ~0.68 PW) to account for the potential effect of increased atmospheric CO_2 [*Crowley*, 1993]. The ocean heat transport values used by *Crowley and Baum* [1995] were significantly smaller than the values computed by the OGCM used in this study. In addition, the poleward heat transport averaged at each latitude used in *Crowley and Baum* [1995] was symmetrized and unchanged from the present-day run. The much different geographic configuration characteristic of the Late Ordovician resulted in a spatial redistribution of the heat transport and a significant asymmetry relative to the equator (Figure 6c). These findings question the validity of the use of symmetric (about the equator) prescribed ocean heat transports in previous uncoupled atmosphere/mixed layer ocean modeling studies.

4. Coupled Model Response to Ordovician Radiative Forcing

4.1. Sensitivity to Atmospheric CO_2

The sensitivity of the coupled model to changes in atmospheric CO_2 levels within the Late Ordovician context was investigated by conducting three experiments with concentrations 10x (control), 14x (14x_cfws.1), and 18x pil (18x_cfws.1). These values span the range of uncertainty associated with *Berner*'s [1994] geochemical estimates.

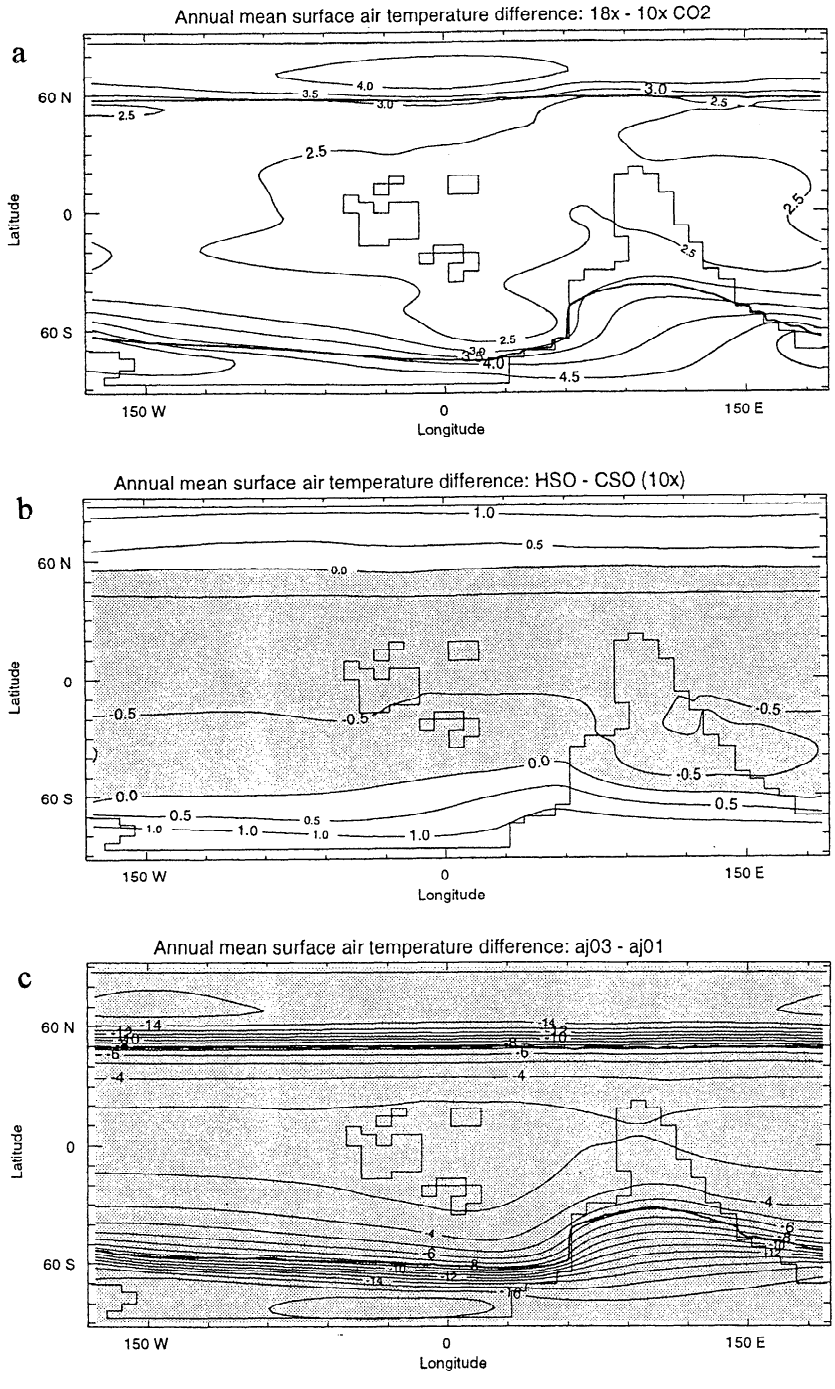

Figure 7. Annual mean SAT (degrees Celsius) difference for (a) 18x – 10x CO_2, (b) hot summer orbit – cold summer orbit, and (c) aj0.3 – aj0.1. Contour intervals are for Figures 7a and 7b 0.5°C and 1.0°C for Figure 7c. The heavy line over the ocean represents the maximum sea-ice extent, whereas over Gondwana it represents the location of the –10.0°C contour or the snow extent (whichever extends the farthest to low latitudes). The ice edge delimits the maximum snow/sea-ice-covered area present during a 1 year period. Shading indicates temperatures below 0°C.

The spatial distribution of the annual mean SAT response to changes in atmospheric CO_2 (18x-10x, Figure 7a) indicates that atmospheric temperatures are quite sensitive to variations in CO_2 forcing. The minimum warming is found in the tropics (~2.5°C), whereas the maximum warming occurs over Gondwana (~5°C) and in the polar latitudes of both hemispheres. The amplification of the difference at high latitudes is due to snow and sea-ice albedo feedbacks. The presence of a large zonal belt of increased atmospheric temperatures bordering the south coast of Gondwana is attributed to the contraction of the Southern Hemisphere sea-ice cover. Both the insulating effect of sea-ice and the albedo feedbacks associated with its reflective surface contribute in the dampening of the response. A similar response is visible

in the Northern Hemisphere along the ice edge. The large temperature increase over Gondwana is connected to snow-albedo-temperature feedbacks.

The effect of atmospheric CO_2 on seasonality is investigated through a latitude versus time distribution of the difference in atmospheric temperature between the 18x and 10x experiments (Figure 8a). The seasonal cycle within the coupled model is driven by changes in solar insolation and by monthly averaged winds. The atmospheric thermal response is accentuated in the polar regions during the winter season when ice-albedo feedback difference would be greatest (Figure 8a). In the Southern Hemisphere, maximum warming is achieved in mid-August, which represents the end of the austral winter and also the time when the ice albedo difference is largest.

The annual global mean SAT increased by 2.7°C between the 10x and 18x experiments, whereas the globally averaged ocean temperature warmed by 0.4°C (Table 1). When compared to an experiment using present-day radiative forcing, orbital forcing, and length of day, these represent an increase of 2.1° and 4.8°C for the 10x and 18x experiments, respectively (Table 2). The globally averaged ocean temperature similarly shows an increase of 0.2° and 0.5°C relative to the present-day experiment for the 10x and 18x experiments, respectively.

The snow cover relative to changes in CO_2 concentrations is assessed through the evaluation of the January average snow cover on Gondwana and sea-ice extent. The month of January is analyzed because it coincides with the end of the austral summer. We assume that snow present during that period has survived through the melt season and is likely to become part of a permanent ice sheet. January snow cover on Gondwana did not survive for any of the CFWS CO_2 sensitivity experiments conducted in this study (Table 1). However, a parallel set of CO_2 sensitivity experiments was performed by changing only the orbital forcing to a WFCS configuration (Table 1: 10x_wfcs.1, 14x_wfcs.1, and 18x_wfcs.1). Although a permanent snow cover did not subsist for the 14x and 18x WFCS experiments, the 10x_wfcs.1 did have a small area of snow (0.17 x 10^6 km^2), which survived in the southern latitudes of Gondwana.

Estimates of Southern Hemisphere sea-ice extent represent January averages, whereas for the Northern Hemisphere, estimates represent July averages as they coincide with the end of the austral and boreal summer, respectively. Sea-ice extent shows a strong dependence on atmospheric CO_2 levels. For the CFWS experiments, Southern Hemisphere sea-ice only survived for the 10x scenario with a January average area of 0.93 x 10^6 km^2 (Table 1). However, for the WFCS CO_2 sensitivity experiments, January sea-ice cover in the Southern Hemisphere survived for the 10x (2.83 x 10^6 km^2), 14x (0.65 x 10^6 km^2), and 18x (0.39 x 10^6 km^2) cases. A large Northern Hemisphere sea-ice extent is present in all experiments (CFWS and WFCS) and reaches a maximum extent of 20.4 x 10^6 km^2 in the 10x_cfws control experiment (Table 1). This sea-ice cover extends down to ~60°N.

There are 145 melting days per year for the 10x experiment, whereas for the 18x experiment, melting takes place for 170 d y^{-1} (Table 3). Assuming a maximum melt rate of 5 cm d^{-1}, this implies that for an ice cap to develop on Gondwana the minimum winter snow depth needs to be > 7.3 m for the 10x (rain equivalent = 2.2 m) and 8.5 m for the 18x (rain equivalent = 2.6 m) in order to exceed the summer melt. To accumulate these amounts of snow during the winter months, precipitation rates should near 3.7 (10x) and 4.9 m yr^{-1} (18x). Present-day precipitation rates rarely exceed ~5 m yr^{-1} except along mountain ranges or coastal areas. It is unlikely that

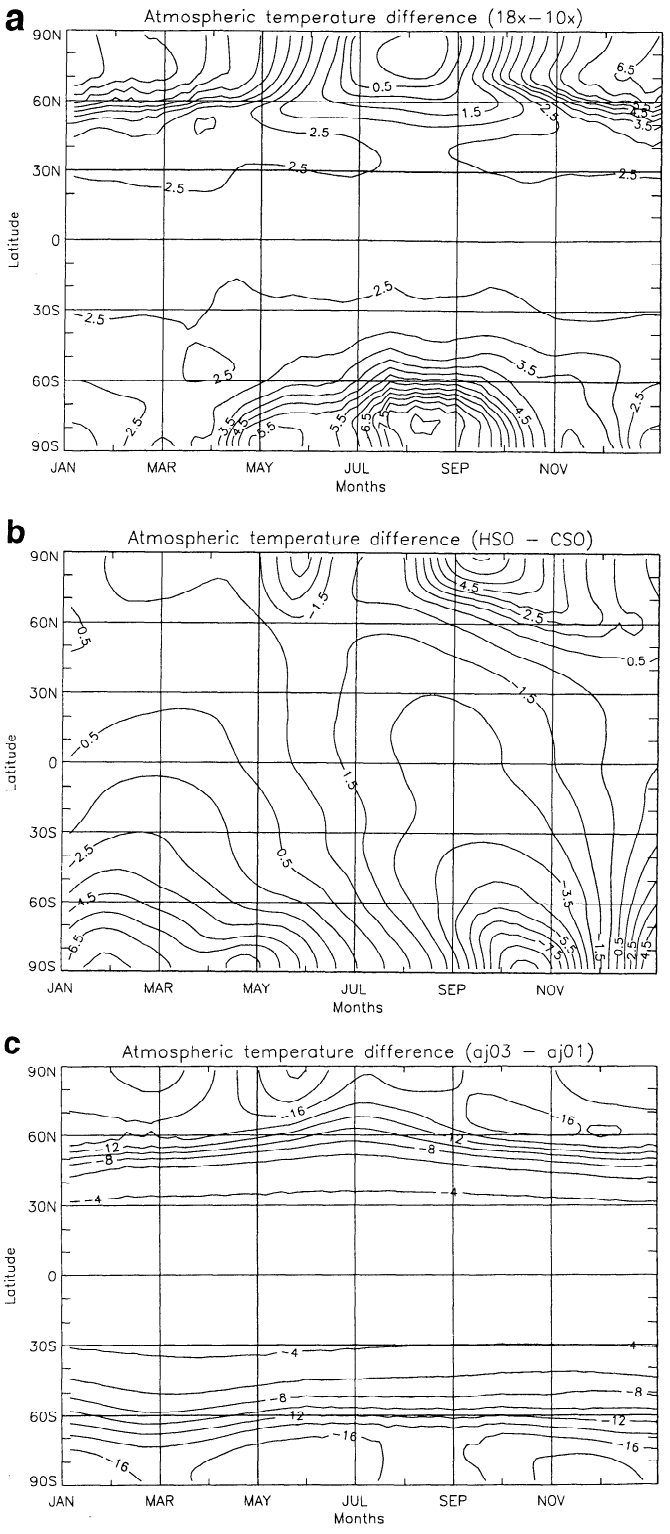

Figure 8. Latitude versus time distribution of the difference in zonal mean SAT (degrees Celsius) between (a) 18x – 10x, (b) hot summer orbit – cold summer orbit, and (c) aj0.3 – aj0.1. Contour intervals are 0.5°C for Figure 8a, 1.0°C for Figure 8b, and 2.0°C for Figure 8c.

Table 2. Climatc Sensitivity Parameters

CO_2 Relative to pil, ppm	ΔForcing, W m^{-2} ΔCO_2	−4.5% sl	Net Forcing, W m^{-2}	ΔT_a Relative to 1x_pdo.1, °C	ΔT_o Relative to 1x_pdo.1, °C
280 (1x)	-1.3	-10.8	-12.1	---	---
2800 (10x)	12.0	-10.8	1.2	2.1	0.2
3920 (14x)	13.9	-10.8	3.1	3.8	0.5
5040 (18x)	15.4	-10.8	4.6	4.8	0.5

For the 1x_pdo.1 experiment we used present-day radiative forcing, orbital forcing, and length of day and prescribed a Latc Ordovician geography; pil is preindustrial levels, and sl is solar luminosity.

precipitation rates would be this high in the interior of Gondwana. The maximum difference in atmospheric temperatures occurs during the austral winter when sea-ice and snow covers are at their maximum extent (up to 8.5°C, Figure 8a). Thc annual mean polar temperature for the 10x is -14.7°C and is −10.0°C for the 18x experiment (Table 3).

4.2. Model Sensitivity to Orbital Parameters

We now present an analysis of the sensitivity of the coupled model to changes in orbital parameters within the Late Ordovician context. To this end we consider two extreme orbital configurations CSO and HSO. The annual mean insolation receipt at the top of the atmosphere depends on the eccentricity and hence does not vary between the CSO and the HSO experiments. However, the latitudinal profile of the zonally averaged annual insolation shows marked differences between the two configurations. While polar latitudes receive an annual surplus of solar insolation by as much as 16.5 W m^{-2} for the HSO compared to CSO, the equatorial and tropical latitudes receive less insolation in the HSO compared to the CSO (up to 4 W m^{-2}). The climatic response to the spatial variations in insolation (Figure 7b) shows that the annual SAT field strongly depends on the solar insolation forcing. Equatorial and tropical SATs are ~0.5°C cooler, whereas polar temperatures are ~1°C warmer for the HSO configuration. Maximum warming occurs in polar latitudes of both hemispheres where the difference in annual solar radiation is the largest. Although changes in the orbital forcing influence the spatial distribution of atmospheric temperatures, results show no major changes on annually averaged global ocean and atmospheric temperatures (Table 1). The absence of a global thermal response is explained by the fact that the annual insolation receipt is not altered significantly between the two configurations.

The theory of the ice ages relies on the idea that summer temperatures play the critical role in glacial inception. Whereas high-latitudc winter temperatures are always cold enough to ensure precipitation to fall as snow, summer temperatures can be warm enough so as to prevent the development of a permanent snow cover. In fact, *Crowell* [1978] argued that summer temperatures play a more significant role in glacial inception than the supply of moisture. Model results show that the intensity of the seasonal cycle is accentuated in the HSO experiment and diminished in the CSO experiment (Figure 8b). An analysis of the seasonal cycle provides a means for determining the critical summer temperature for which glacial inception is still possible. When summer temperatures are too hot, the development of a permanent ice cap is not possible. October polar SATs are ~9.5°cooler for the HSO experiment, whereas February SATs are ~7.5°C warmer for the Southern Hemisphere (Figure 8b). Although temperature extremes are greater for the HSO configuration, the annually averaged polar temperature is ~1°C cooler for the CSO because of the presence of a permanent snow cover (Table 3). In addition, summer temperatures never rise above freezing for the CSO experiment. Following the argument presented by *Crowley et al.* [1987], with annual precipitation rates as low as 10 cm and below freezing summer temperatures, a 1000 m thick ice sheet could be produced within the relatively short time of 10,000 years. On the other hand, extremely high snow precipitation during the winter season would not survive through a long and intense melt season.

The modeled permanent snow/sea-ice cover, relative to

Table 3. Climatic Indicators for Glacial Inception on the South Pole

Experiment	Annually Averaged Polar Temperature, °C	Length of Melt Season, days
10x	-14.7	145
18x	-10.0	170
Aj0.1	-15.0	135
Aj0.3	-31.6	0
HSO	-13.4	150
CSO	-14.7	145

Experiment names represent the following runs: 10x, control; 18x, 18x_cfws.1; Aj0.1, 10x_wfcs.1; Aj0.3, 10x_wfcs.3; hot summer orbit (HSO), 10x_hso.1; and cold summer orbit (CSO), 10x_cso.1.

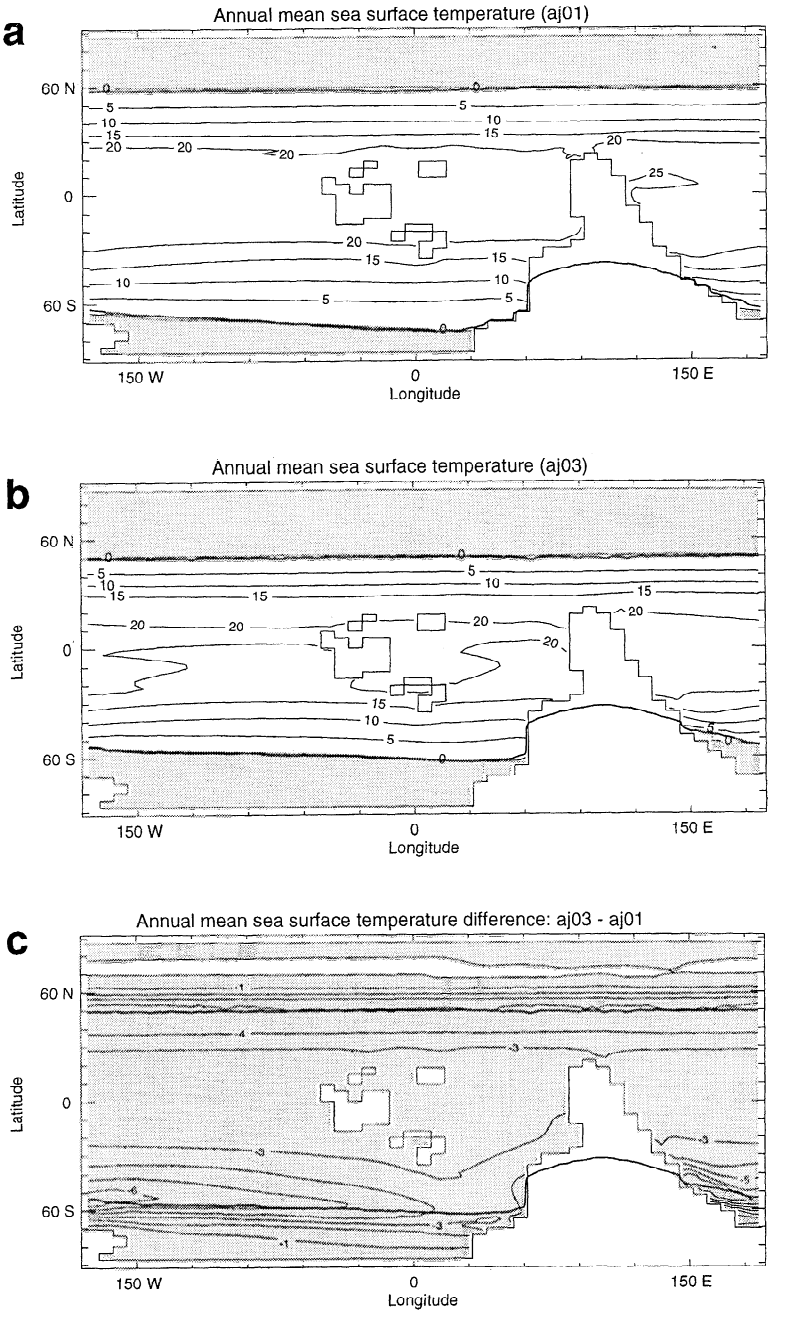

Figure 9. Annual mean SST (degrees Celsius) distributions for (a) aj0.1 and (b) aj0.3 experiments. Contour intervals are 5°C. The heavy line over the ocean represents the maximum sea-ice extent, whereas over Gondwana it represents the location of the −10.0°C contour or the snow extent (whichever extends the farthest to low latitudes). The ice edge delimits the maximum snow/sea-ice-covered area present during a 1 year period. (c) Annual mean SST (degrees Celsius) difference between the aj0.3 and aj0.1 experiments. The heavy line is the ice edge for the aj0.3 experiment, and the contour intervals are 1°C. Shading indicates temperatures below 0°C in Figures 9a and 9b.

changes in orbital forcing, reflected the decrease in incoming solar radiation at high latitudes for the CSO experiment and resulted in an increase of the snow cover and sea-ice extent. The spatial increase of highly reflective surfaces produced a further decrease in absorbed solar radiation, resulting in a further cooling. This explains why the thermal response was amplified at high latitudes through this positive feedback loop. The extent of sea-ice in the southern high latitudes (January average) increased from 0.65 x 10^6 km^2 for the HSO to 2.90 x 10^6 km^2 for the CSO configuration. There was no permanent snow cover for the HSO experiment, whereas for the CSO the modeled snow cover was 0.54 x 10^6 km^2. The extent of the Northern Hemisphere sea-ice cover was maximum for the HSO experiment (21.4 x 10^6 km^2) as the configuration corresponds to a CSO configuration for the Northern Hemisphere.

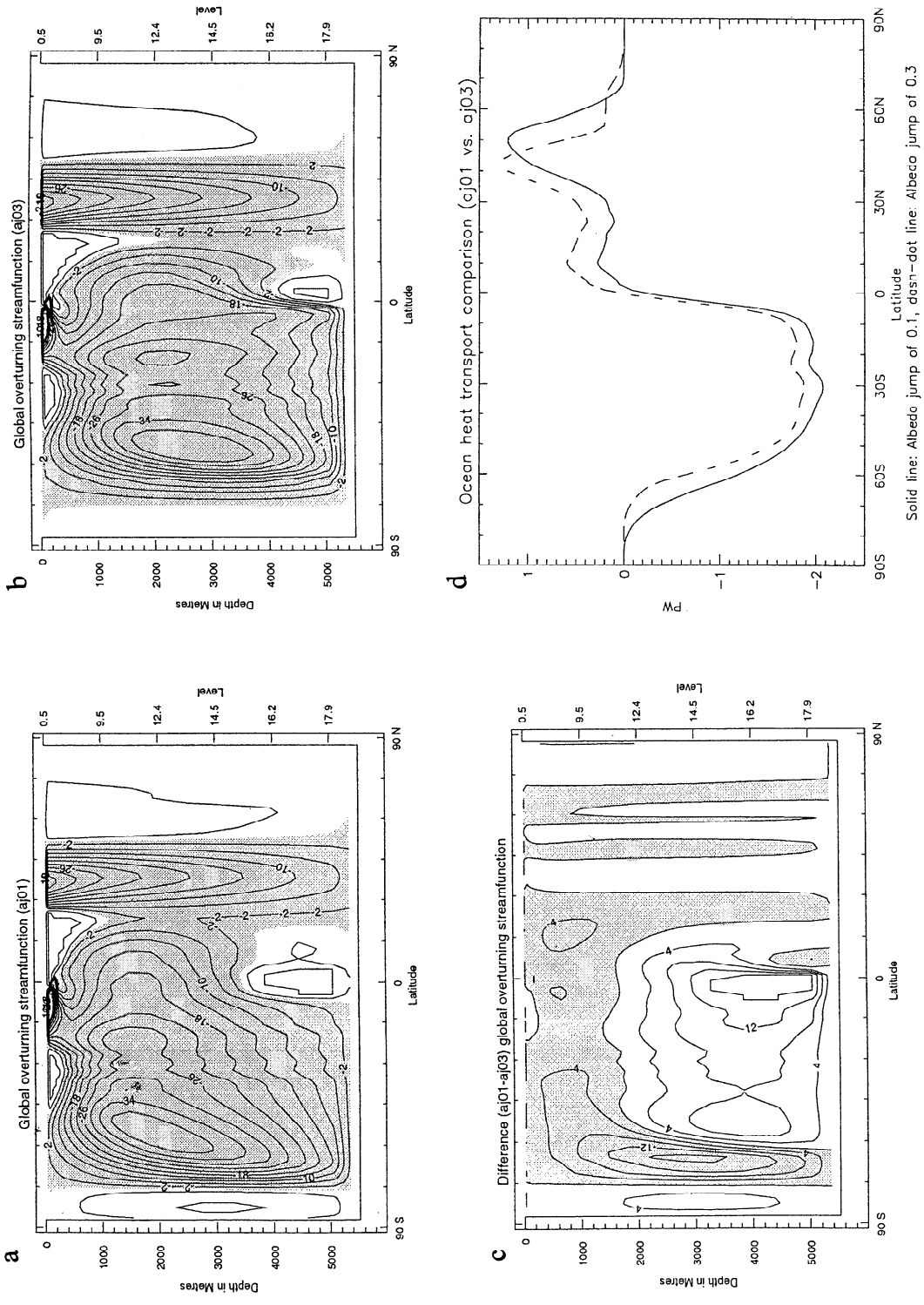

Figure 10. Global overturning stream function for (a) aj0.1 and (b) aj0.3, and (c) difference in global overturning stream function (Sv) between the aj0.1 and aj0.3 experiments. Contour intervals are 4 Sv. (d) Global ocean heat transport comparison in PW between aj01 (solid line) and aj0.3 (dash-dot line). Shading indicates a counterclockwise circulation in Figures 10a and 10c.

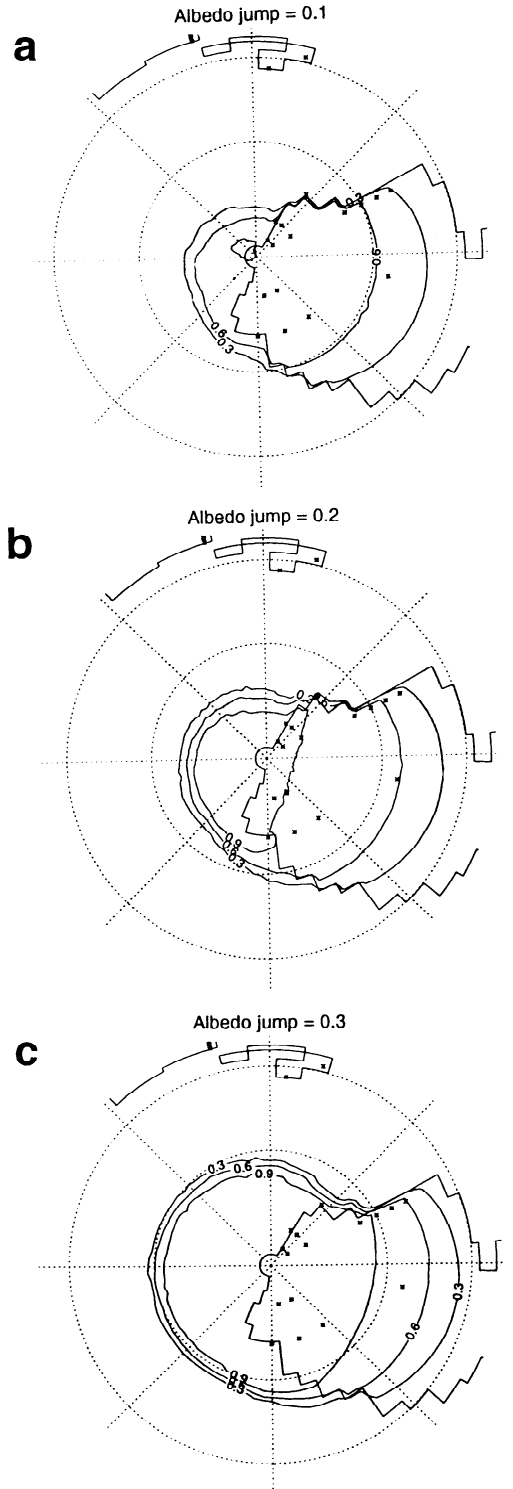

Figure 11. Annually averaged ice/snow concentration over sea/land, respectively, for ice-snow albedo parameters of (a) 0.1, (b) 0.2, and (c) 0.3. Contour intervals are 0.3, and asterisks represent an approximate distribution of glacial deposits [*Paris et al.*, 1995].

4.3. Model Sensitivity to Sea-ice/Snow Albedo Feedback Parameter

Sensitivity of the coupled model to changes in the ice-snow albedo feedback parameter was tested for three possible local reductions to the planetary coalbedo (0.1, 0.2, and 0.3) [*North et al.*, 1983; *Graves et al.*, 1993]. Results show a strong response of the climate model to changes in the ice-snow albedo parameter (Table 1). The annual global mean ocean temperature decreased by 0.8°C and the SAT decreased by 5.9°C between the aj0.1 and aj0.3 experiments. The cooling occurs throughout the year and is enhanced at high latitudes where snow/ice-covered surfaces are present (Figure 8c). Maximum cooling in the southern high latitudes takes place during the winter months (May-June-July) and summer months (November-December-January) when differences in snow/ice-covered areas are the largest and solar insolation reaches its extremes (Figure 8c). SATs remain below −10.0°C (the temperature above which melting occurs in the model) throughout the year for the aj0.3 experiment, whereas the aj0.1 experiment has a melting season of 135 days (Table 3). The averaged temperature during the melt season for the aj0.1 experiment is −2.2°C, whereas it is −3.6°C for the CSO experiment. The fact that summer temperatures are slightly warmer for the aj0.1 experiment than for the CSO may in part explain why the snow and sea-ice accumulation is more important in the latter.

The ice edge in the northern high latitudes expanded 10° equatorward between the aj0.1 and aj0.3 experiments because of the enhanced snow/ice albedo effect (Figures 9a and 9b, heavy line). The difference in the annual mean SST between the aj0.3 and aj0.1 experiments (Figure 9c) shows a cooling over all latitudes except for the Northern Hemisphere high latitudes where permanent sea-ice is present in both experiments. Equatorial and subtropical SSTs cooled by ~2°C. The largest cooling is found along the southeastern coast of Gondwana. This region, which was warmed by the western boundary Antarctica Current in the aj0.1 experiment, is permanently covered by sea-ice in the aj0.3 experiment.

The ocean circulation also shows a strong sensitivity to changes in the ice-snow albedo parameter (Figure 10). Experiments reveal an equatorward shift of the locations of deep water formation with a higher ice-snow albedo parameter (Figures 10a and 10c). In addition, the overturning shows a marked deepening and strengthening below 2000 m with an increased ice-snow albedo parameter. However, a comparison of the global ocean heat transport between the two sensitivities (Figure 10d) shows a decrease in the poleward heat transport in the Southern Hemisphere and north of 35°N with an increased ice-snow albedo parameter. In the Southern Hemisphere, where there exists a meridional land barrier, the overturning is the most dominant mechanism for oceanic heat transport. In general, ocean heat transport is calculated following the temperature difference between poleward surface waters and equatorward flowing subsurface waters. It is possible that the observed reduction in heat transport originates from the reduction of this vertical temperature gradient (as surmized from Figures 9a and 9b).

The sea-ice extent adjacent to the South Pole increased from 2.83 x 10^6 km^2 in the aj0.1 run to 17.70 x 10^6 km^2 in the aj0.3 run, whereas the January average snow cover on Gondwana increased from 0.17 x 10^6 to 14.50 x 10^6 km^2 (Table 1). This value alone, excluding the sea-ice area, represents 123% of the estimated ice sheet. Clearly, the results from the increased ice-snow albedo parameter support the notion of sustained glaciated conditions in the southern high latitudes of Gondwana under 10x atmospheric CO_2 concentrations. In terms of annually averaged sea-ice and land snow

concentrations (Figure 11) the area inclusive of all glacial deposits is snow covered 60% of the year for aj0.3, whereas for the aj0.1 experiment this area is only fully covered 30% of the year.

5. Discussion

There is no direct evidence for a Northern Hemisphere ice cap contemporary to the Late Ordovician glaciation [*Brenchley*, 1988], partly since no cratonic areas were located in the northern high latitudes. However, because of the absence of land masses in the Northern Hemisphere, the modeled meridional circulation is very weak thereby enhancing the isolation of the northern polar latitudes from the equatorial source of heat. Consequently, results from all sensitivity experiments consistently reveal the presence of permanent sea-ice cover extending from the pole to 60°-70°N. A minimum sea-ice extent (at the end of boreal summer) is achieved in the 18x_wfcs.1 experiment with a value of 12.3 x 10^6 km^2, whereas a maximum is achieved in the 10x_wfcs.3 experiment with a value of 59.4 x 10^6 km^2. For comparison, present-day Southern Ocean maximum sea-ice area is ~15 x 10^6 km^2 [*Hartmann*, 1994]. The presence of an extensive permanent sea-ice cover must have affected the biological production in polar latitudes, but the lack of land in these latitudes renders the assessment of its implication difficult.

Geochemical isotopic excursions derived from the Ordovician geologic record suggest an array of possible time frames for the glaciation, the shortest one being ~1 m.y. Clearly, if the glaciation was indeed brief, several orbital configurations could still have been involved during the length of the event. Hence our use of an intermediate configuration to examine the average climate produced under the specified set of parameters is justified. It is also possible that an extreme orbital configuration could have played a preconditioning role for the creation of a glacial climate nearing the end of the Ordovician.

As previously argued by *Crowell* [1978], summer temperatures may play a more critical role in glacial inception than the supply of moisture. Model results showed that whereas high-latitude winter temperatures were always cold enough to ensure precipitation to fall as snow, summer temperatures were in some instances, such as for the HSO, warm enough so as to prevent the development of a permanent snow cover. Perhaps sustained ice albedo feedbacks, concurrent with the existence of an ice sheet, would be sufficient to inhibit the termination of the glaciation when orbital forcing would enter an HSO configuration. The inclusion of a thermomechanical ice sheet model to a coupled OGCM-EMBM would allow this to be tested further by avoiding the shortcomings of the presently used simple snow parameterization.

There are a number of uncertainties associated with this study. The CO_2/radiative effect relationship used here is based on present-day estimates and may not be applicable for concentrations as high as 10-18x pil. *Crowley and Baum*'s [1995] estimate was based on *Kiehl and Dickinson* [1987] and represents, for the 10x CO_2 case, a ~3.0 W m^{-2} increase relative to that calculated from *Ramanathan* [1987]. As this question is clearly still unresolved, further studies are needed in order to improve the radiative estimates. The latitudinal planetary albedo profile may also have differed from the present-day estimate because of changes in land-sea distribution, land surface cover, and cloud cover [*Jenkins et al.*, 1993]. At present the albedo curves generated through Ordovician AGCM experiments account for land-sea effects but do not include particular land surface cover effects such as variations in soil types and presence of large water masses on the continents. In addition, they do not account for potential changes in cloud cover due to the shorter length of day or different geography.

6. Conclusion

Results from the modeling experiments show that it is possible to maintain a substantial permanent snow cover in the southern high latitudes of Gondwana given 10x CO_2 concentrations, WFCS forcing, a 4.5% reduction in solar luminosity, a length of day of 21.5 hours, and an ice-snow albedo parameter of 0.3. The single most important internal parameter, which determines whether a permanent snow cover existed or not, is the magnitude of the ice-snow albedo feedback. In addition, the CSO experiment with 10x CO_2, a decreased solar luminosity and shortened length of day, and an ice-snow albedo parameter of 0.1 also sustained a permanent (albeit less extensive) snow cover. These findings reinforce conclusions previously derived from AGCM experiments as their permanent snow cover is sustained under similar boundary conditions.

The geographic configuration of the Late Ordovician, which was drastically different than that of present-day, resulted in an up to ~42% increase in the global ocean poleward heat transport in the Southern Hemisphere, a latitudinal redistribution of the ocean heat transport, and a significant asymmetry relative to the equator. Future Ordovician AGCM modeling studies should therefore include ocean heat transport values directly calculated by an OGCM, such as the ones obtained in this study. In light of the restraints and uncertainties associated with this study the coupled model was able to produce a permanent snow cover on Gondwana, which included 60% of all the glacial deposits found on the supercontinent.

Acknowledgments. We thank T. Crowley and S. Baum for providing the land-sea mask and M. Gibbs for the wind fields used in the experiments. We are grateful to them as well as M. Eby and A. Fanning for discussions and suggestions linked to this work. C. Poulsen, M. Gibbs, and an anonymous reviewer are thanked for their constructive reviews. This research was supported by an FCAR Fellowship awarded to PFP and by NSERC, CSHD, AES/CICS, and Steacie operating grants, as well as an IBM SUR grant awarded to AJW. All numerical computations were conducted locally on a suite of IBM RS6000s including two SP2s. Infrastructure support from the University of Victoria is gratefully acknowledged.

References

Bahcall, J. N., Solar models, neutrino experiments, and helioseismology, *Rev. Mod. Phys.*, *60*, 297-372, 1988.

Barnes, C. R., The faunal extinction event near the Ordovician-Silurian boundary: A climatically induced crisis, in *Global Bio-Events*, edited by O. Walliser, pp. 121-126, Springer-Verlag, New York, 1986.

Berger, A. L., Long-term variation of caloric insolation resulting from the Earth's orbital elements, *Quat. Res.*, *9*, 139-167, 1978.

Berger, A. L., M. F. Loutre and V. Dehant, Influence of the changing lunar orbit on the astronomical frequencies of pre-Quaternary insolation patterns, *Paleoceanography*, *4*, 555-564, 1989.

Berner, R. A., 3GEOCARB II: A revised model of atmospheric CO_2 over Phanerozoic time, *Am. J. Sci.*, *294*, 56-91, 1994.

Beuf, S., B. Biju-Duval, O. de Carpal, P. Rognon, O. Gariel and A. Bennacef, Les grès du Paléozoique inférieur au Sahara: Sédimentation et discontinuités, évolution structurale d'un craton, *Publ. Inst. Fr. Pet. Tech.*, *18*, 1-464, 1971.

Brenchley, P. J., Environmental changes close to the Ordovician-Silurian boundary, *Bull. Br. Mus. Nat. Hist.*, *43*, 377-385, 1988.

Brenchley, P. J. and G. Newall, Late Ordovician environmental changes and their effect on faunas, in *Aspects of the Ordovician System*, edited by D. L. Bruton, pp. 65-79 , Univ. of Oslo, Oslo, Norway, 1984.

Brenchley, P. J., G. A. F. Carden and J. D. Marshall, Environmental changes associated with the "first strike" of the Late Ordovician mass extinction, *Mod. Geol.*, *20*, 69-82, 1995.

Caputo, M V., Ordovician-Silurian glaciations and global sea-level changes, in *Silurian Cycles: Linkages of Dynamic Stratigraphy With Atmospheric, Oceanic, and Tectonic Changes*, edited by E. Landing and M. E. Johnson, pp. 15-26 , New York State Educ. Dep., New York, 1998.

Caputo, M. V. and J. C. Crowell, Migration of glacial centers across Gondwana during Paleozoic Era, *Geol. Soc. Am. Bull.*, *96*, 1020-1036, 1985.

Crowell, J. C., Gondwana glaciations, cyclotherms, continental positioning and climatic change, *Am. J. Sci.*, *278*, 1345-1372, 1978.

Crowley, T. J., Geological assessment of the greenhouse effect, *Bull. Am. Meteorol. Soc.*, *74*, 2363-2373, 1993.

Crowley, T. J., J. G. Mengel and D. A. Short, Gondwanaland's seasonal cycle, *Nature*, *329*, 803-807, 1987.

Crowley, T. J. and S. K. Baum, Toward reconciliation of Late Ordovician (~440 Ma) glaciation with very high CO_2 levels, *J. Geophys. Res.*, *96*, 22,597-22,610, 1991.

Crowley, T. J. and S. K. Baum, Reconciling Late Ordovician (440 Ma) glaciation with very high (14X) CO_2 levels, *J. Geophys. Res.*, *100*, 1093-1101, 1995.

Endal, A. S. and S. Sofia, Rotation in solar-type stars, I, Evolutionary models for the spin-down of the sun, *Astrophys. J.*, *243*, 625-640, 1981.

Fanning, A. F. and A. J. Weaver, An atmospheric energy-moisture balance model: Climatology, interpentadal climate change, and coupling to an ocean general circulation model, *J. Geophys. Res.*, *101*, 15,111-15,128, 1996.

Fanning, A. F. and A. J. Weaver, Temporal-geographical meltwater influences on the North Atlantic conveyor: Implications for the Younger Dryas, *Paleoceanography*, *12*, 307-320, 1997.

Frakes, L. A., J. E. Francis and J. I. Syktes, *Climate Modes of the Phanerozoic*, 274 pp., Cambridge Univ. Press, New York, 1992.

Gibbs, M. T., E. J. Barron and L. R. Kump, An atmospheric pCO_2 threshold for glaciation in the Late Ordovician, *Geology*, *25*, 447-450, 1997.

Graves, C. E., W. Lee and G. R. North, New parameterizations and sensitivities for simple climate models, *J. Geophys. Res.*, *98*, 5025-5036, 1993.

Hambrey, M. J., The Late Ordovician-Early Silurian Glacial Period, *Palaeogeogr., Palaeoclimatol.,Palaeoecol.*, *51*, 273-289, 1985.

Hambrey, M. J. and W. B. Harland, *Earth's Pre-Pleistocene Glacial Record*, 1004 pp., Cambridge Univ. Press, New York, 1981.

Hartmann, D. L., *Global Physical Climatology*, 411 pp., Academic, San Diego, Calif., 1994.

Hibler, W. D., A dynamic thermodynamic sea ice model, *J. Phys. Oceanogr.*, *9*, 815-846, 1979.

Houghton, H. G., *Physical Meteorology*, 442 pp., Mass. Inst. of Technol., Cambridge, 1985.

Hyde, W. T., K. Kim and T. J. Crowley, On the relation between polar continentality and climate: Studies with a nonlinear seasonal energy balance model, *J. Geophys. Res.*, *95*, 18,653-18,668, 1990.

Jenkins, G. S., H. G. Marshall and W. R. Kuhn, Precambrian climate: The effects of land area and Earth's rotation rate, *J. Geophys. Res.*, *98*, 8785-8791, 1993.

Kasting, J. F., Paradox lost and paradox found, *Nature*, *355*, 676-677, 1992.

Kiehl, J. T. and R. E. Dickinson, A study of the radiative effects of enhanced atmospheric CO_2 and CH_4 on early Earth surface temperatures, *J. Geophys. Res.*, *92*, 2991-2998, 1987.

Levitus, S. and T. P. Boyer, *World Ocean Atlas 1994: Temperature*, 117 pp., Washington, D.C., NOAA, 1994.

Marshall, J. D., P. J. Brenchley, P. Mason, G. A. Wolff, R. A. Astini, L. Hints and T. Meidla, Global carbon isotopic events associated with mass extinction and glaciation in the Late Ordovician, *Palaeogeogr., Palaeoclimatol.,Palaeoecol.*, *132*, 195-210, 1997.

Middleton, P. D., J. D. Marshall and P. J. Brenchley, Evidence for isotopic change associated with Late Ordovician glaciation, from brachiopods and marine cements of central Sweden, in *Advances in Ordovician Geology*, edited by C. R. Barnes and S. H. Williams, *Pap. Geol. Surv. Can. 90-9*, 313-323 , 1991.

Newman, M. J. and R. T. Rood, Implications of solar evolution for the Earth's early atmosphere, *Science*, *198*, 1035-1037, 1977.

North, G. R., J. G. Mengel and D. A. Short, Simple energy balance model resolving the seasons and the continents: Application to the astronomical theory of the ice ages, *J. Geophys. Res.*, *88*, 6576-6586, 1983.

Pacanowski, R., MOM 2 documentation user's guide and reference manual, in *technical report*, pp. 232, Geophys. Fluid Dyn. Lab. Ocean Group, Princeton, N.J., 1995.

Paris, F., Z. Elaouad-Debbaj, J. C. Jaglin, D. Massa and L. Oulebsir, Chitinozoans and Late Ordovician glacial events on Gondwana, in *Ordovician Odyssey: Short Papers for the 7th International Symposium on the Ordovician System*, edited by J. D. Cooper, M. L. Droser and S. L. Finney, pp. 171-176, Pacific Section Society for Sedimentary Geology, Fullerton, Calif., 1995.

Ramanathan, V., The role of Earth radiation budget studies in climate and general circulation research, *J. Geophys. Res.*, *92*, 4075-4095, 1987.

Ramanathan, V., et al., Climate-chemical interactions and effects of changing atmospheric trace gases, *Rev. Geophys.*, *25*, 1441-1482, 1987.

Ross, J. R. P. and C. A. Ross, Ordovician sea-level fluctuations, in *Global Perspectives on Ordovician Geology*, edited by B. D. Webby and J. R. Laurie, pp. 327-335 , A. A. Balkema, Brookfield, Vt., 1992.

Scotese, C. R. and J. Golonka, *Paleogeographic Atlas, Paleomap Project*, Univ. of Tex., Arlington, 1992.

Scrutton, C. T., Periodic growth features in fossil organisms and the length of the day and the month, in *Tidal Friction and the Earth's Rotation*, edited by P. Brosche and J. Sundermann, pp. 154-196 , Springer-Verlag, New York, 1978.

Semtner, A. J., A model for the thermodynamic growth of sea ice in numerical investigations of climate, *J. Phys. Oceanogr.*, *6*, 379-389, 1976.

Sepkoski, J., Jr., Patterns of Phanerozoic extinction: A perspective from global data bases, in *Global Events and Event Stratigraphy in the Phanerozoic*, edited by O. H. Walliser, pp. 35-51 , Springer-Verlag, New York, 1995.

Sonett, C. P., S. A. Finney, and C. R. Williams, The lunar orbit in the Late Precambrian and the Elatina sandstone laminae, *Nature*, *335*, 806-808, 1988.

Sonett, C. P., E. P. Kvale, A. Zakharian, M. A. Chan and T. M. Demko, Late Proterozoic and Paleozoic tides, retreat of the moon, and rotation of the Earth, *Science*, *273*, 100-104, 1996.

Thompson, S. L. and D. Pollard, A global climate model (GENESIS) with a Land-Surface Transfer Scheme (LSX), I, Present climate simulation, *J. Clim.*, *8*, 732-761, 1995.

Underwood, C. J., S. F. Crowley, J. D. Marshall and P. J. Brenchley, High-resolution carbon isotope stratigraphy of the basal Silurian stratotype (Dob's Linn, Scotland) and its global correlation, *J. Geol. Soc.*, *154*, 709-718, 1997.

Veizer, J., et al., $^{87}SR/^{86}SR$, $\delta^{18}O$ evolution of Phanerozoic seawater, *Chem. Geol.*, in press, 1999.

Wang, K., B. D. E. Chatterton, M. Attrep and C. J. Orth, Late Ordovician mass extinction in the Selwyn Basin, northwestern Canada: Geochemical, sedimentological, and paleontological evidence, *Can. J. Earth Scien.*, *30*, 1870-1880, 1993.

Wang, K., B. D. E. Chatterton and Y. Wang, An organic carbon isotope record of Late Ordovician to Early Silurian marine sedimentary rocks, Yangtze Sea, South China: Implications for CO_2 changes during the Hirnantian glaciation, *Palaeogeogr., Palaeoclimatol.,Palaeoecol.*, *132*, 147-158, 1997.

Weaver, A. J., M. Eby, A. F. Fanning and E. C. Wiebe, Simulated influence of carbon dioxide, orbital forcing and ice sheets on the climate of the Last Glacial Maximum, *Nature, 394*, 847-853, 1998.

Weaver, A. J. and T. M. C. Hughes, On the incompatibility of ocean and atmosphere models and the need for flux adjustments, *Clim. Dyn., 12*, 141-170, 1996.

Wiebe, E. C. and A. J. Weaver, On the sensitivity of global warming experiments to the parameterisation of sub-grid scale ocean mixing, *Clim. Dyn.*, in press, 1999.

Wilde, P., Oceanography in the Ordovician, in *Advances in Ordovician Geology*, edited by C. R. Barnes and S. H. Williams, *Pap. Geol. Surv. Can. 90-9*, 283-298 , 1991.

Williams, D. M., J. Harkin and A. H. N. Rice, Umbers, ocean crust and the Irish Caledonides: terrane transpression and the morphology of the Laurentian margin, *J. Geol. Soc. London, 154*, 829-838, 1997.

Yapp, C. J. and H. Poths, Ancient atmospheric CO_2 pressures inferred from natural goethites, *Nature, 355*, 342-344, 1992.

C. R. Barnes, P. F. Poussart, and A. J. Weaver, School of Earth and Ocean Sciences, University of Victoria, P.O. Box 3055, Victoria, British Columbia, Canada V8W 3P6. (crbarnes@uvic.ca; poussart@ocean.seos.uvic.ca; weaver@ocean.seos.uvic.ca)

(Received December 15, 1998;
revised April 1, 1999;
accepted April 4, 1999.)